Journal of
Virology and Infectious Diseases

ScienceAssist International

Research Article | Open Access

In Silico Analysis and Computational Assessment of Potential Inhibitors of SARS-Cov-2 Main Protease

Riyan Al Islam Reshad[1], Md. Hazrat Ali[1], Chandrashekhar Ghosh[2], Md. Zahidul Akram Ratul[2], Mowaz Mohammed Abdul Karim[3], Ali Wahab Showhardo[1], S.M Yousuf Uddin[1], Samriddha Majumdar[1], Md. Tanvir Ahmed[1], Md. Akkas Ali[1]*

[1]Department of Genetic Engineering and Biotechnology, Shahjalal University of Science and Technology, Sylhet, Bangladesh
[2]Department of Computer Science and Engineering, Shahjalal University of Science and Technology, Sylhet, Bangladesh
[3]Department of Civil and Environmental Engineering, Shahjalal University of Science and Technology, Sylhet, Bangladesh

***Correspondence:** Ali A, Department of Genetic Engineering and Biotechnology, Shahjalal University of Science and Technology, Sylhet, Bangladesh. E-mail: akkas-geb@sust.edu

Received: January 27, 2021; Accepted: February 24, 2021; Published: March 03, 2021

Abstract

Severe Acute Respiratory Syndrome Coronavirus 2 (SARS-CoV-2) outbreak in China has caused so many deaths with a significant number of confirmed cases around the world. This virus's highly contagious nature has raised the scientific community's concern to find a cure to treat coronavirus disease (COVID-19) caused by the viral infection. In this study 1615, FDA approved ligand structures were analyzed to identify the best possible therapeutic inhibitor(s) for SARS-CoV-2 main protease. Upon sequential computational experiments, Lindane (Induced Fit Docking; IFD Score: -594.02 Kcal/mol), Gluconolactone (IFD Score: -585.77 Kcal/mol), and Mitoxantrone (IFD Score: -582.33 Kcal/mol) were found to be the best inhibitors of SARS-CoV-2 main protease. Then these compounds were analyzed in different post-screening experiments where they were also observed to perform well. This study will contribute to the current efforts of scientific society to secure treatment for COVID-19. However, further in vivo and in vitro experiments might be required to properly validate the findings of this study.

Keywords: Coronavirus; COVID-19; Deaths; Inhibitors; Main Protease

INTRODUCTION

Coronavirus is a type of pathogen that causes potentially deadly diseases in mammals and birds [1]. In humans, they may cause severe to mild respiratory, enteral, hepatic, or neurologic diseases with symptoms of fever, cough, and shortness of breath [2]. They are enveloped single-stranded, positive-sense RNA viruses. It is currently known as the largest RNA genome and is phenotypically and genotypically diverse [3].

Coronavirus resides in the family Coronaviridae (genera-coronavirus and torovirus) in the order nidovirales [4]. They are widely spread in bats worldwide and found in many other species such as birds, dogs, pigs, mice, cats, and humans [5]. Members of the coronavirus family possess a large genome that ranges from 27-32 kb. This coronavirus genome encodes for 5/ replicase polyprotein containing two reading frames ORFs 1a and 1b, which in order, encodes for all the enzymes necessary for viral RNA replication [6].

According to serology and genome phylogeny, coronaviruses are classified into four genera, termed Alpha, Beta, Delta, and Gramma coronavirus [7]. So far, seven human coronaviruses have been identified, containing two alpha CoVs (HCoV-229E and HCoV-NL63) and five beta CoVs (HCoV-OC43, HCoV-HKU1, severe acute respiratory syndrome CoV (SARS-CoV), middle east respiratory syndrome CoV (MERS-CoV) and most recent SARS-CoV-2 [8].

In the 1960s [9], two human coronaviruses- human coronavirus 229E (HCoV- 229E) and human coronavirus OC43 (HCoV-OC43) were known to infect humans [10] in the lower respiratory tract [11]. After this, a third human coronavirus, SARS-CoV, was discovered responsible for severe acute respiratory syndrome [12]. It was first identified in November 2002, in China's Guangdong region [13,14]. The world health organization (WHO) declared that the disease was spread to 29 areas worldwide in 2003. Eight thousand ninety-eight individuals were infected, and among them, 774 death cases were observed [15]. After the SARS epidemic,

the two other human coronaviruses, HCoV-NL63 and HCoV-HKU1 were discovered quickly. On 23 September 2012, the WHO found a new coronavirus- middle east respiratory syndrome coronavirus (MERS-CoV). In 2012 and December 2019, 2465, MERS-CoV infection cases were confirmed, and 850 deaths were reported from 27 countries to the WHO [10-16].

However, these two highly pathogenic coronaviruses (SARS-CoV and MERS-CoV) caused global epidemics with terrifying morbidity and mortality. In December 2019, another human coronavirus outbreak, causing the COVID-19, was recorded in Wuhan City, Hubei Province, China. According to epidemiological studies, this outbreak was associated with Wuhan's seafood market [17,18]. Based on phylogenetic analysis of the complete viral genome (29,903 nucleotides), it was demonstrated that SARS-CoV-2 was most nearly related (89.1% nucleotides similarity) to the SARS-like coronavirus [19].

And the protein sequences of SARS-CoV-2 main protease (CMP) and SARS-CoV main protease have 96.1% sequence identity (Figure 1).

Viral main protease processes other viral precursor proteins for proper functioning, and therefore blocking their activity is an effective strategy in developing antiviral drugs [22,23]. In this study, a total of 1615 FDA approved compounds were docked against SARS-CoV-2 main protease. The sequential computational analysis led to identifying the best three compounds that were then utilized in another post-screening study (Figure 2).

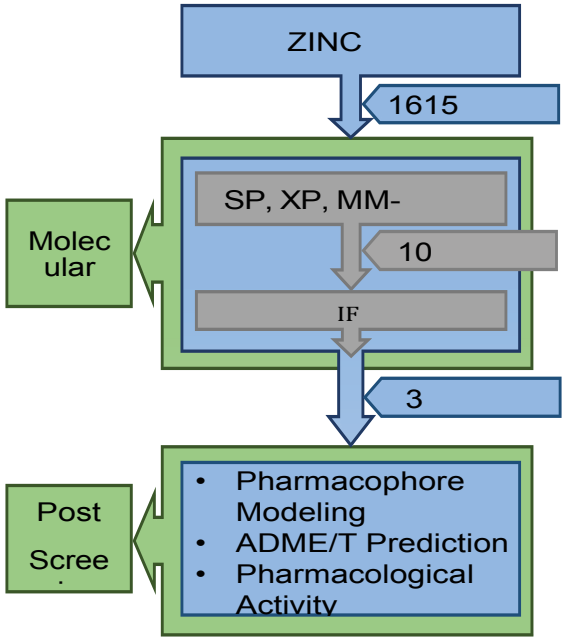

Figure 2: Strategies employed in the overall study.

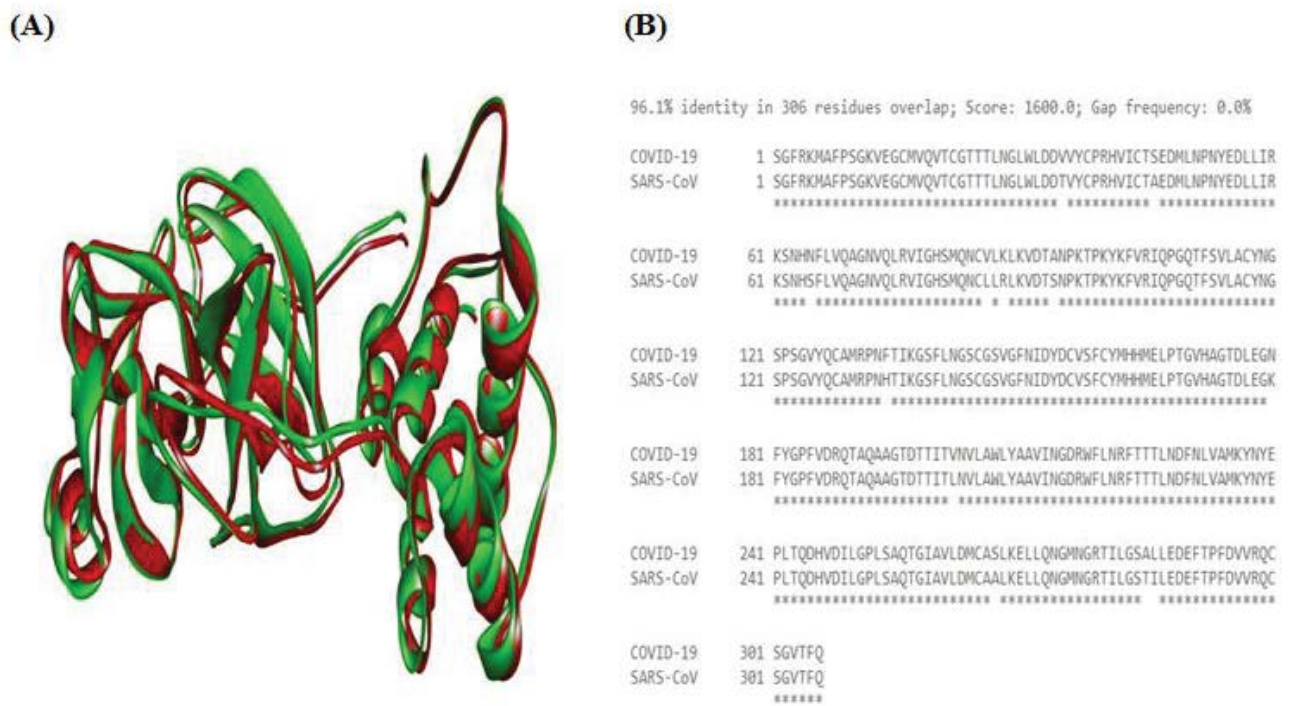

Figure 1: (A) Superimposition of SARS-CoV-2 main protease (Red; PDB Id: 6LU7) and SARS- CoV main protease (Green; PDD Id: 2H2Z) [20,21]. (B) Alignment of SARS-CoV-2 and SARS- CoV main protease protein sequences.

MATERIALS AND METHODS

Molecular Docking

Protein preparation

PDB format of SARS-CoV-2 main protease (SMP) (PDB ID: 67U7) was downloaded from Protein Data Bank (www.rcsb.org) in the three-dimensional crystallographic form [24], which has an inhibitor protein attached to its active site. To prepare and process Protein Preparation Wizard's protein structure in Maestro Schrödinger Suite (v11.4) was used. Assigning the bond orders to the structures, hydrogens were added to the heavy atoms. All of the water molecules were erased from the atoms; missing side chains were adjusted in the protein structure backbone using Prime as well as het states were generated with Epik at pH 7 ± 2 [25]. Optimized Potentials for Liquid Simulations force field (OPLS_2005) in the suite was utilized, setting the RMSD (root-mean- square-deviation) to 30 Å to refine and minimize the protein structure. Any extraordinary water under 3H-bonds to non-water was erased in the minimization step.

Ligand preparation

A total of 1615 FDA approved drug (ligand) structures were downloaded in sdf format from ZINC database (https://zinc.docking.org/) [26]. LigPrep wizard of Maestro Schrödinger suite was used to prepare and process these ligand structures [27]. Minimized 3D structures of the ligands were generated using Epik2.2 within pH 7.0 +/- 2.0 in the suite. Finally, minimization was carried out again using the OPLS_2005 force field, which generated maximum 32 possible stereoisomers depending on available chiral centers on each molecule.

Receptor grid generation

Receptor grid was generated using default Van der Waals radius scaling factor 1.0 and charge cutoff 0.25, which was then subjected to the OPLS_2005 force field for the minimized structure in Glide [28]. The grid generated a cubic box around the active site (co-crystallized reference ligand) of the target molecules. Finally, the grid box dimension was then adjusted to 14 Å ×14 Å×14 Å for docking to be carried out.

Glide standard precision (SP) and extra precision ligand docking

To compare docking parameters, both Extra precision (XP) ligand docking and Standard precision (SP) ligand docking methods are used that are suitable and accurate for small number and the large number of ligand molecules, respectively [29,30]. To carry out docking of the ligand molecules, Van der Waals radius scaling factor 0.80 and charge cutoff 0.15 were set, which assigned final scores according to the docked ligand's pose within the binding cleft of the receptor molecule. Discovery Studio Visualizer (v4.5) was utilized to analyze the best possible poses and types of ligand-receptor interactions [31].

Prime MM-GBSA rescoring

The ligands were subjected to Molecular mechanics-generalized born and surface area (MM- GBSA) rescoring with Prime module of Maestro Schrödinger suite for further evaluation after SP XP ligand docking. MM-GBSA assigns a more accurate scoring function, which in turn improves the overall free binding affinity score upon the reprocessing of the docked ligand to the biological macromolecules by the utilization of an implicit solvent [32-34]. This technique generally combines OPLS molecular mechanics energies (EMM), surface generalized born solvation model for polar solvation (GSGB), and a nonpolar salvation term (GNP) for total free energy (ΔGbind) calculation. The following equation calculated the total free energy of binding:

ΔGbind = Gcomplex – (Gprotein – Gligand), where, G= EMM + GSGB + GNP

Induced fit docking

Ten best compounds with the lowest MM-GBSA scores were selected for further evaluation since it is the more robust scoring method. To obtain more accurate docking result, the chosen ligand molecules were subjected to induced fit docking (IFD) that generates the native poses of the ligands bound to its target [32-35]. After having generated a grid around the receptor's co- crystallized ligand structure, the OPLS_2005 force field was applied again, and the five best ligands were docked rigidly. Van der Waals screening for the receptor (0.70) and ligand (0.50) was set, residues within 2 Å were refined in order to generate the two best possible posses with the standard precision method.

Structure-based Pharmacophore Modeling

Pharmacophore modeling is one of the essential tools used for successful drug discovery. It is usually used for both lead identification and lead optimization and aids in the prompt understanding of 2D or 3D level identity of molecules by schematically depicting the critical elements of molecular recognition [36,37]. 3D structure-based pharmacophore modeling was obtained using LigandScout 4.4.1 Essential [38]. LigandScout

autonomously generates pharmacophore features like- hydrogen bond donors, hydrogen bond acceptors, hydrophobic, positive and negative ionizable, aromatic interactions, and 3D geometries of the intended bioactive molecules using an advanced algorithm [39].

ADME/T Prediction

In silico prediction of the ADME/T profile of candidate drug molecules, it helps pharmaceutical industries select the best candidates, which reduces the time and cost of the drug discovery approach [40-42]. ADME/T profile for three selected ligand molecules (Table 3) that performed well in the docking experiment was analyzed using an online based server, i.e., admetSAR 2.0 (http://lmmd.ecust.edu.cn/admetsar2) and pkCSM (http://biosig.unimelb.edu.au/pkcsm/prediction) to predict different pharmacokinetic and pharmacodynamic properties. These are including blood- brain barrier permeability, human abdominal absorption, AMES toxicity, Cytochrome P (CYP) inhibitory promiscuity, carcinogenicity, mutagenicity, and Caco-2 permeability [43,44].

PASS (Prediction of Activity Spectra for Substances) Prediction

Prediction of Activity Spectra for Substances (PASS) estimates the tentative biological activities of query compounds based on their native chemical structure. PASS predicts the action of a compound based on Structure-Activity Relationship Base (SAR Base), which assumes that the activity of a compound is related to its structure. It works by comparing the 2D structure of a compound relative to another compound having biological activities recorded in the database with almost 95% accuracy [45]. Probable antiviral activities and other intended activities against proteins involved in mediating viral infection of the selected molecules were predicted using PASS online server (http://www.pharmaexpert.ru/passonline/) [46].

DFT (Density Functional Theory) Calculation

DFT calculation was carried out by using minimized ligand structures from LigPrep. This calculation theory uses the Jaguar panel of Maestro Schrödinger Suite, which uses Becke's three- parameter exchange potential as well as Lee-Yang-Parr correlation (B3LYP) theory with 6-31G* basis set [47-50]. Different quantum chemical properties such as surface properties (MO, density, potential) and Multipole moments were calculated along with HOMO (Highest Occupied Molecular Orbital) and LUMO (Lowest Unoccupied Molecular Orbital) energy. Then the global frontier orbital was analyzed as well as hardness (η) and softness (S) of selected molecules were calculated using the following equation as per Parr and Pearson interpretation and Koopmans theorem [51,52]. The DFT calculation result is summarized in Table 6, and the HOMO and LUMO occupation of the ligands is illustrated in.

$\eta = (HOMO\mathcal{E} - LUMO\mathcal{E})/2$, $S = 1/\eta$

RESULTS

Molecular Docking Study

Among all the ligand molecules used in SP, XP, and MM-GBSA scoring, 10 molecules were selected based on the lowest binding free energies since it is the most rigorous scoring method mentioned earlier (Table 1). Three best performing ligand molecules were selected based on the IFD scores, which is considered a more accurate way of predicting binding poses than SP and XP from 10 selected molecules that showed slight variation between SP and XP docking scores. These three ligand molecules were Lindane, Gluconolactone, and Mitoxantrone (Table 2), and these ligands were found to exhibit the lowest IFD scores (Table 3). As a result, these compounds were utilized for further study, and others were opted out from further consideration.

Table 1: Result of SP and XP docking and free binding energy calculation.

Compound ID	SP Docking Score (Kcal/mol)	XP Docking Score (Kcal/mol)	Glide Ligand Efficienc y	Glid e ecoul	Glide evdw	Glide energ y	MM- GBSA ΔGbind (Kcal/mol)
ZINC00000381086 0	-6.749	-5.328	-0.078	-1.34	- 30.03 3	- 31.370	-77.03
ZINC00024520492 4	-5.874	-4.751	-0.313	- 1.227	- 21.85 3	- 23.080	-64.07
ZINC00002130321 0	-5.775	-4.460	-0.204	0.166	- 33.03 4	- 32.868	-62.14
ZINC00000253970 2	-5.214	-4.134	-0.067	- 4.317	-41.32	- 45.637	-61.05
ZINC00001970230 9	-5.689	-5.123	-0.258	- 0.352	-31.93	- 32.282	-59.59
ZINC00000089659 5	-4.893	-4.477	-0.213	-3.45	- 26.94 3	- 30.393	-54.25
ZINC00000379479 4	-5.683	-4.172	-0.264	- 1.985	- 23.89 9	- 25.884	-53.43
ZINC00000000043 1	-6.085	-4.956	-0.236	- 5.536	- 34.79 2	- 40.328	-53.18
ZINC00000640973 5	-5.116	-4.111	-0.316	0.987	- 27.32 1	- 26.334	-52.77
ZINC00000395288 1	-5.261	-3.853	-0.148	- 2.888	- 34.79 6	- 37.684	-45.96

Table 2: The results of induced fit docking between the best performing ligands and SMP.

Compound ID	Compound Name	MM- GBSA ΔGbind (Kcal/mol)	Glide Gscore (Kcal/mol)	IFD Score (Kcal/mol)	Interacting Amino Acids	Bond Distance (Å)	Type of Interaction	Interaction Category
ZINC000245204924	Lindane	-64.07	-6.25	-594.02	Cys145	4.80	Alkyl	Hydrophobic
					Met49	4.75	Alkyl	Hydrophobic
					Cys145	5.22	Alkyl	Hydrophobic
					Met49	5.30	Pi-Alkyl	Hydrophobic
					Met165	3.67	Alkyl	Hydrophobic
					His41	5.11	Pi-Pi T Shaped	Hydrophobic
					Met165	5.48	Pi-Alkyl	Hydrophobic
					His41	2.92	Hydrogen Bond	Non-conventional
					Met165	4.92	Alkyl	Hydrophobic
					His41	4.15	Pi-Alkyl	Hydrophobic
					Arg188	3.09	Chlorine Interaction	Halogen
					His41	3.65	Pi-Alkyl	Hydrophobic
					Met49	3.30	Alkyl	Hydrophobic
ZINC000002539702	Gluconolactone	-61.05	-3.97	-585.77	His41	4.77	Pi-Pi T Shaped	Hydrophobic
					Glu166	2.27	Hydrogen Bond	Conventional
					His41	2.78	Hydrogen Bond	Non-conventional
					Arg188	2.59	Hydrogen Bond	Non-conventional
					Met49	4.95	Pi-Alkyl	Hydrophobic
ZINC000003794794	Mitoxantrone	-53.43	-3.38	-582.33	Met165	2.95	Pi-Alkyl	Hydrophobic
					His41	2.70	Hydrogen Bond	Conventional
					Ser144	2.71	Hydrogen Bond	Conventional
					Asn142	2.85	Hydrogen Bond	Non-conventional
					Gly143	2.04	Hydrogen Bond	Conventional

Binding mode of lindane with SARS-CoV-2 main protease (SMP)

Lindane is one of the selected best performance showing ligand molecules that interacted with 5 amino acids within the binding pocket and formed a total of 6 interactions when docked with SMP with a better IFD score (-594.02 Kcal/mol) as well as Glide Gscore (-6.25 Kcal/mol) (Table 2). It formed one non-conventional hydrogen bond with His41 amino acid residue at 2.92 Å distance apart, one Pi-Pi T shaped interaction with His41, and one halogen interaction with Arg188 amino acid residue. It also formed additional hydrophobic interactions, i.e., Alkyl and Pi-Alkyl interactions with Cys145, Met49, Met165 amino acid residues within the binding cleft of CMP (Figure 3).

Binding mode of gluconolactone with SARS-CoV-2 main protease (SMP)

Gluconolactone is another best performance showing ligand molecule that generated an IFD score of -585.77 Kcal/mol and Glide Gscore of -3.97 Kcal/mol to dock with SMP and formed total 6 interaction when interacted with 4 amino acids within the binding pocket (Table 2). It formed one conventional hydrogen bond with Glu166 amino acid residue at 2.27 Å distance apart and two non-conventional interactions with His41 and Arg188 amino acid residues at 2.78 and 2.59 Å distance apart,

Table 3: Best performed ligand molecules in the overall molecular docking experiment.

Zinc ID	Compound Name	IUPAC Name	Chemical Formula	2D structure
ZINC0002452 04924	Lindane	1,2,3,4,5,6- hexachlorocyclohexane	$C_6H_6Cl_6$	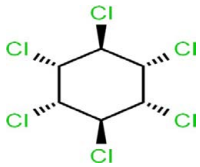
ZINC0000025 39702	Gluconolactone	(3*R*,4*S*,5*S*,6*R*)-3,4,5-trihydroxy-6-(hydroxymethyl)oxan-2-one	$C_6H_{10}O_6$	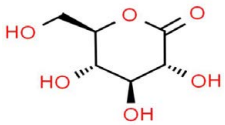
ZINC0000037 94794	Mitoxantrone	1,4-dihydroxy-5,8-bis[2-(2-hydroxyethylamino)ethylamino] anthracene-9,10-dione	$C_{22}H_{28}N_4O_6$	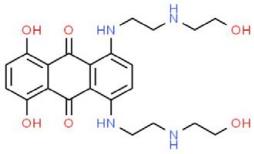

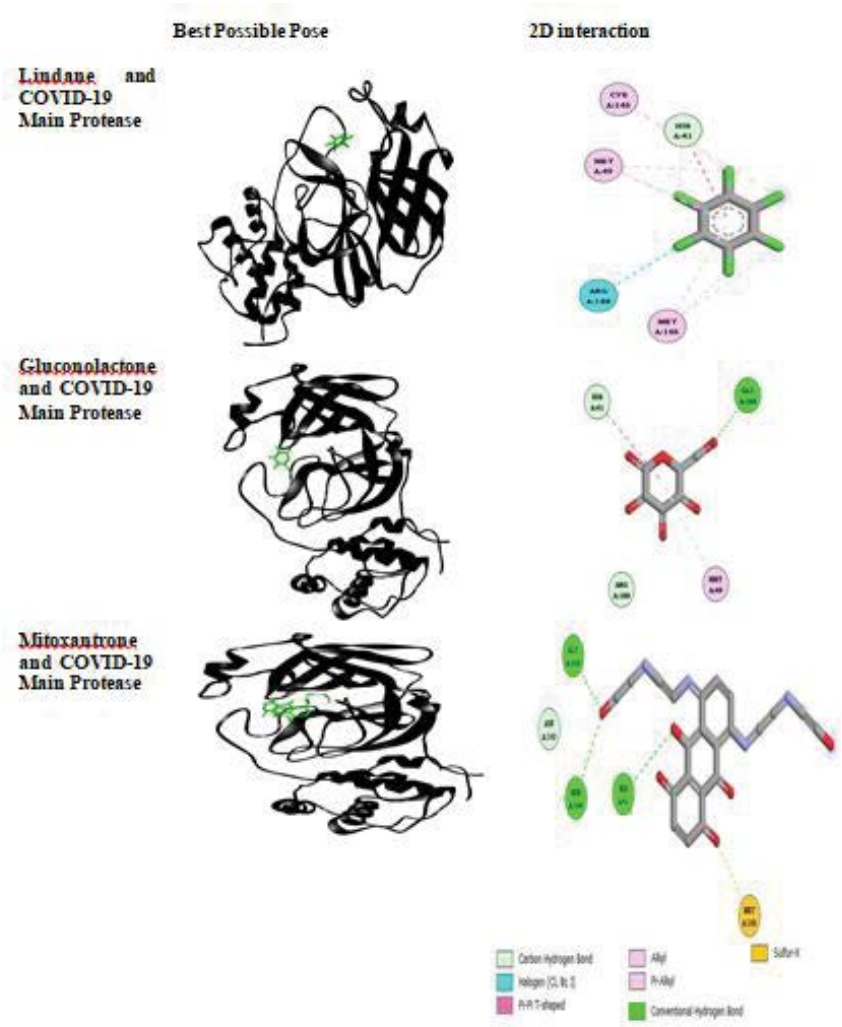

Figure 3: Representation of best possible poses (left) and ligand-receptor interactions (right) between the docked complexes.

respectively. Additional hydrophobic Pi-Alkyl interaction was also formed with Met49 amino acid residue within the binding cleft of CMP (Figure 4).

Binding mode of mitoxantrone with SARS-CoV-2 main protease (SMP)

Mitoxantrone generated an IFD score of -582.33 Kcal/mol and Glide Gscore of -3.38 Kcal/mol to dock with SMP and formed a total 6 interactions interacting with 4 amino acids (Table 2). It formed three conventional hydrogen bonds with His41, Ser144, and Gly143 amino acid residue at 2.70, 2.71, and 2.04 Å distance apart. Moreover, Mitoxantrone also created one non-conventional hydrogen bond interaction with Asn142 amino acid residue at 2.85 Å distance apart, respectively. Again, it formed additional hydrophobic Pi-Alkyl interactions with Met165 amino acid residue within the binding cleft of SMP (Figure 4).

Pharmacophore Modeling

The result of pharmacophore modeling is represented in (Figure 4). Lindane was reported to show only hydrophobic features, and Met165 and Met49 amino acid residues were shown to contribute to the bond formation with the pharmacophoric quality. Gluconolactone formed three hydrogen bond donor features and one hydrogen bond acceptor feature, and His41, Met165, and Glu166 amino acid residues were shown to contribute to the bond formation with the pharmacophoric features. Again, Mitoxantrone formed three hydrogen bond donor features within the binding site of CMP.

ADME/T Prediction

ADME/T (absorption, distribution, metabolism, excretion, and toxicity) profile was analyzed for all selected ligand molecules, and the results are summarized in (Table 4). The best three selected ligand molecules (Lindane, Gluconolactone, and Mitoxantrone) showed high oral bioavailability. Lindane has higher Caco2 cell line permeable capability compare to Gluconolactone

Table 4: Results of ADME/T tests of best selected ligands. OCT2: Organic Cation Transporter 2; *hERG:* Human ether-a-go-go related gene, CYP: Cytochrome P450

Properties	Lindane	Gluconolactone	Mitoxantrone
Absorption			
Human intestinal absorption	High	Low	High
Human oral bioavailability	High	High	High
Caco-2 permeability	High	Low	Low
Distribution			
P-glycoprotein substrate	No	No	Yes
P-glycoprotein inhibitor	No	No	No
Blood-brain barrier penetration	Yes	Yes	No
Metabolism			
CYP3A4 substrate	No	No	No
CYP2C9 substrate	No	No	No
CYP2D6 substrate	No	No	No
CYP3A4 inhibition	No	No	No
CYP2C9 inhibition	No	No	No
CYP2D6 inhibition	No	No	No
Excretion			
Total clearance	1.053	0.678	1.424
OCT2 substrate	No	No	No
Toxicity			
AMES toxicity	No	No	Yes
Hepatotoxicity	No	No	Yes
hERG inhibition	No	No	No
Eye irritation	Yes	No	No
Acute oral toxicity	III	IV	III

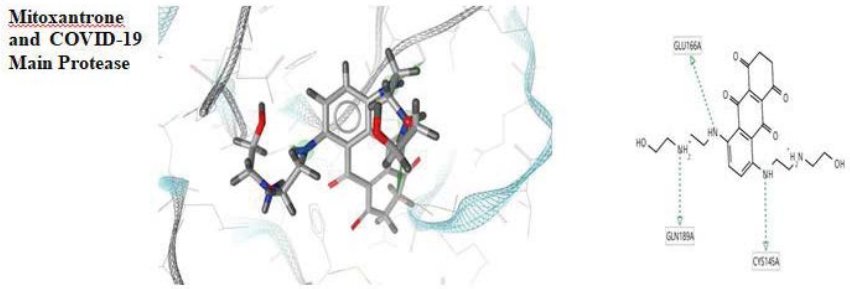

Figure 4: Three dimensional (left) and Two dimensional (right) representation of structure-based pharmacophore modeling between selected ligand molecules and SMP. Hydrogen bond donor, hydrogen bond acceptor, and hydrophobic features are represented as green, red, and yellow.

and Mitoxantrone, respectively. Gluconolactone showed less human intestinal absorption, whereas Lindane Mitoxantrone's absorption rate was high. Plasma membrane protein, P-glycoprotein, was not inhibited by any of the best-selected ligand molecules; Mitoxantrone acted as a substrate. Lindane and Gluconolactone showed the blood-brain permeable capability, but none of the ligands showed the sign as either inhibitor or substrate of CYP3A4, CYP2D6, CYP2C9, and OCT2. None of them was reported to be substrates of OCT2 (Organic Cation Transporter 2). Mitoxantrone was predicted to have Ames toxicity and hepatotoxicity, whereas Lindane was shown to induce eye irritation. On the contrary, Mitoxantrone and Lindane showed type III acute oral toxicity, and Gluconolactone showed type IV.

Pharmacological Activity Prediction

In order to determine the association of ligand molecules with other antiviral activities based on their native structures, their pharmacological activities were predicted, and the result is represented in Table 5. Gluconolactone showed better antiviral activity against different viruses and other actions against different enzymes involved in viral infection mediation. However, Mitoxantrone was predicted to have moderate activity followed by Lindane.

Analysis of Frontier's Orbitals

Detailed HOMO energy, LUMO energy, energy gap (HOMO-LUMO gap), hardness, and softness of the selected best compounds are summarized in Table 6, and the HOMO and LUMO occupation of the ligand molecules is illustrated in (Figures 5 and 6) for each compound. The highest energy gap was predicted for Lindane, and the lowest gap was observed for Mitoxantrone.

According to the energy gap, the stability order of the compounds is: Mitoxantrone>Gluconolactone>Lindane. Along with the HOMO and LUMO energy, each compound's dipole moment was also calculated, and based on the dipole moments, the molecules' stability order is Mitoxantrone>Lindane>Gluconolactone.

DISCUSSION

Due to the utilization of specific algorithms and scoring function as well as the particular pose of ligand-receptor interaction, molecular docking is the most commonly used drug discovery approach by the researchers [53,54]. In this experiment 1615, FDA-approved ligand structures were downloaded from the ZINC database, and then they were subjected to SP, XP, and binding free energy calculation. Out of them, 10 best performing ligand molecules were selected based on their lowest binding energy, reflecting the higher affinity of ligand molecules

Table 5: Result of Pharmacological Activity prediction of selected ligand molecules. Pa>0.7: Compound is very likely to have activity; Pa>0.5: Compound is expected to have activity

Activities	Lindane		Gluconolacton e		Mitoxantrone	
	Pa	Pi	Pa	Pi	Pa	Pi
Antiviral (Picornavirus)	0.546	0.033	0.704	0.005	-	-
Antiviral (Poxvirus)	0.373	0.034	0.678	0.011	0.348	0.040
Simian immunodeficiency virus proteinase inhibitor	0.525	0.016	0.466	0.029	0.286	0.138
Antiviral (Adenovirus)	0.391	0.033	0.407	0.026	0.441	0.016
Antiviral (Influenza)	0.265	0.116	0.687	0.006	0.334	0.071
Antiviral (Herpes)	0.429	0.024	0.512	0.008	0.318	0.079
Antiviral (Hepatitis B)	-	-	0.478	0.005	0.166	0.143
Antiviral	0.375	0.018	0.361	0.021	-	-
Antiviral (Rhinovirus)	-	-	0.437	0.057	-	-
RNA-directed RNA polymerase inhibitor	0.438	0.030	0.484	0.013	-	-
RNA directed DNA polymerase inhibitor	0.503	0.009	0.408	0.017	0.213	0.076
HIV-2 reverse transcriptase inhibitor	0.305	0.009	0.185	0.041	0.207	0.031
3C-like protease (Human coronavirus) inhibitor	0.297	0.027	0.231	0.108	-	-

Table 6: Result of DFT calculation. The unit of HOMO, LUMO, gap, hardness, and softness are in Hartree, and the unit of dipole moment is in Debye.

Compound Name	HOMO	LUMO	Gap	Hardness (η)	Softness (S)	Dipole Moment
Lindane	-0.30473	-0.03623	0.2685	0.13425	7.4487	2.2069
Gluconolactone	-0.27343	-0.02362	0.24981	0.124905	8.0060	4.6608
Mitoxantrone	-0.17629	-0.08850	0.08779	0.043895	22.8003	2.0253

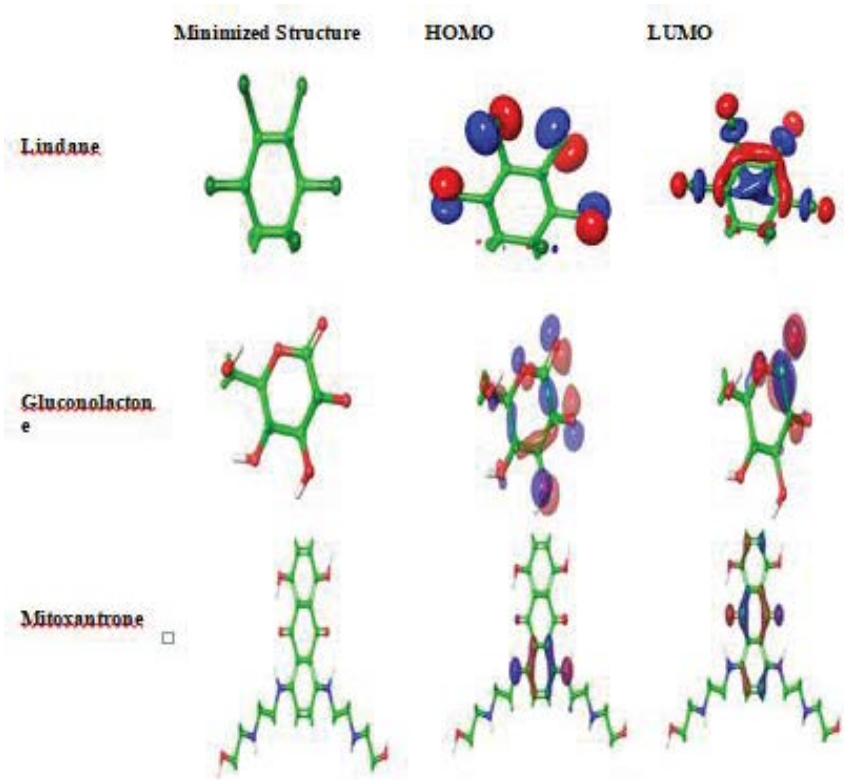

Figure 5: The HOMO and LUMO occupation for the selected compounds. Blue and red is positive and negative in their wave function.

for their receptors. The selected ligand molecules were again subjected to induced fit docking (IFD) to obtain a more accurate docking result (Table 1). Based on the induced-fit docking experiment scores, Lindane, Gluconolactone, and Mitoxantrone were selected as the best inhibitors of SMP, and their drug-like potentials were then evaluated (Tables 2 and 3). In this study, Lindane, Gluconolactone, and Mitoxantrone showed the lowest binding energies and formed multiple numbers of hydrogen bonds and hydrophobic interactions within the binding site of SMP (Figure 3). These interactions are significant for serving biological purposes, making the ligand-receptor complex more efficient [55,56].

In SARS Coronavirus main protease His41 and Cys145 amino acid residues form the catalytic dyad of the enzyme's active site [57]. In our study, the best-selected ligand molecules formed hydrogen bonds and hydrophobic interaction with either His41 or Cys145 amino acid residue of the active site of CMP. They thus predicted to interfere with the normal function of the protease. Pharmacophore modeling is a fascinating technique for de novo drug designing and lead optimization. Structure-based pharmacophore modeling uses a 3D structure of a macromolecular target or a target-ligand complex to predict pharmacophoric features of the complex. As a part of the protocol subsequently, structure-based pharmacophore modeling utilizes an assessment of the complementary chemical features of the binding site and their spatial orientation relationships, which results in a pharmacophore model assembly with selected features, i.e., hydrogen bond donors, hydrogen bond acceptors, and hydrophobes [58,59]. The best-docked compounds were reported to have significant hydrogen bond donors, acceptors, and hydrophobic features (Figure 4).

Considering the most concerning issues such as blood-brain barrier permeability for drugs that usually target cells of the central nervous system (CNS), determining the most efficient route of drugs, the highly absorbed organs or tissues, the ADME/T (absorption, distribution, metabolism, excretion, and toxicity) profile of drugs is analyzed during the development of a potential drug [60,61]. Plasma membrane proteins such as P-glycoproteins play a significant role in the side human body's drug transport mechanism. Human intestinal tissue permeability of a drug is ensured by the Caco2 cell line permeability of that drug [62-64]. Inside the human body, drug interaction, metabolism, and drug excretion outside the body are regulated by the Cytochrome P450

family of enzymes. Inhibition of these enzymes leads to the normal process's impairment and may cause acute drug toxicity, slow clearance, and malfunction of drugs [65,67]. AMES toxicity parameter is used to examine the toxicity endpoint of chemicals under investigation [68,69]. hERG (Human ether-a-go-go related gene) channels are the voltage-gated potassium ion channels that play crucial roles for potassium ion transport through the cell membrane, and this hERG potassium channel can be blocked by structurally and functionally different as well as unrelated drugs that may raise off-target drug interaction. To minimize the undesirable drug interaction, compounds for hERG channels are screened during the early lead optimization process [70]. The substrates of Renal OCT2 (organic cation transporter 2) are readily excreted through urine, and this transporter is essential for drugs and xenobiotic excretion through the kidney [71]. Lindane was predicted to have better ADME/T profiles than the other two molecules (Table 4).

Pharmacological activity (PASS prediction) refers to the Probability of activity (Pa) and the Probability of inactivity (Pi) of a compound, and the result of the forecast ranges from 0.000 to 1.000. The activity of a compound can only be possible When Pa>Pi [72]. A compound is considered highly active when its Pa value is greater than 0.7 (Pa>0.7), and there is a possibility of that compound being analog to a known pharmaceutical agent is also high. A compound also shows activity when its Pa value is greater than 0.5 but less than 0.7 (0.5<Pa<0.7), but the possibility of being analogue to a known pharmaceutical agent is low, and when a compound has Pa value less than 0.5 (Pa<0.5), it is considered as a less active compound [73]. The selected compounds were analyzed to determine the antiviral activities and activities against proteins and enzymes involved in viral infection, and Gluconolactone was predicted to have better pharmacological activities than other selected molecules (Table 5). The HOMO-LUMO gap defines a compound's stability, and HOMO refers to a constraint portion in a molecule capable of donating electrons, whereas LUMO is responsible for accepting electrons. To determine the stability of the best selected ligand molecules, their HOMO and LUMO energy were analyzed (Figure 5). It is required for a compound to have the highest gap to undergo a chemical reaction more efficiently [74,75]. Lindane was predicted to have a more positive energy gap than other molecules (Table 6). Finally, upon continual computational exploration, Lindane, Gluconolactone, and Mitoxantrone were identified as the best inhibitors of SARS-CoV-2 main protease. Lindane performed slightly better than the other two ligand molecules in different post- screening studies. This study recommends that Lindane, Gluconolactone, and Mitoxantrone be the best SMP inhibitors that could be directed against SARS-CoV-2 infection. These compounds should also work against SARS coronavirus main protease since both the proteases are structurally almost identical (Figure 1).

However, computational exploration is mostly based on the modeling of the molecules and sometimes may come out with faulty outcomes, although the growing techniques have increased its fidelity of prediction, and these techniques have become famous for computer-aided drug designing in the last few decades [76]. So, further laboratory experiments might be required to strengthen the findings of this study.

CONCLUSION

The Wuhan Novel Coronavirus outbreak in China caused many deaths worldwide, and many people got infected just after few days of the outbreak. Finding a cure for this nasty virus has become the primary concern of the scientific community. Our study screened a total of 1615 FDA- approved structures against SARS-CoV-2 main protease and gradually explored Lindane, Gluconolactone, and Mitoxantrone as the best inhibitors of this enzyme. These compounds were then subjected to evaluation in different drug-like parameter defining experiments where they were also performing sound. The authors believe this study will uphold the scientists' efforts to find a cure against SARS-CoV-2 infection. However, the authors suggest further in vivo and in vitro experiments for proper validation of this experiment.

CONFLICT OF INTEREST

The authors declare no conflict of interest regarding the publication of the manuscript.

DATA AVAILABILITY STATEMENT

The authors made all the data generated during the experiment and analysis available within the manuscript.

REFERENCES

1. Weiss SR, Navas-Martin S. Coronavirus pathogenesis and the emerging pathogen severe acute respiratory syndrome coronavirus. Microbiol. Mol Biol Rev. 2005;69(4):635-64.
2. Choi KW, Chau TN, Tsang O, Tso E. Characteristics and outcomes of patients with severe acute respiratory syndrome (SARS) in Hong Kong. Ann Intern Med. 2003;139(9):I15.
3. Ziebuhr J. Molecular biology of severe acute respiratory syndrome coronavirus. Curr Opin Microbiol. 2004;7(4):412-9.
4. Abdul-Rasool S, Fielding BC. Understanding human coronavirus HCoV-NL63. Open Virol J. 2010;4:76.

5. van der Hoek L, Pyrc K, Jebbink MF, Vermeulen-Oost W, Berkhout RJ, Wolthers KC, et al. Identification of a new human coronavirus. Nat Med. 2004;10(4):368-73.

6. Imbert I, Snijder EJ, Dimitrova M, Guillemot JC, Lécine P, Canard B. The SARS-Coronavirus PLnc domain of nsp3 as a replication/transcription scaffolding protein. Virus Res. 2008;133(2):136-48.

7. Araf Y, Faruqui NA, Anwar S, Hosen MJ. SARS-CoV-2: a new dimension to our understanding of coronaviruses. Int Microbiol. 2020; 24:1-6.

8. Zhu Y, Li C, Chen L, Xu B, Zhou Y, Cao L, et al. A novel human coronavirus OC43 genotype detected in mainland China. Emerg Microbes Infect. 2018;7(1):1-4.

9. Marra MA, Jones SJ, Astell CR, Holt RA, Brooks-Wilson A, Butterfield YS, Khattra J, Asano JK, Barber SA, Chan SY, Cloutier A. The genome sequence of the SARS-associated coronavirus. Science. 2003;300(5624):1399-404.

10. Lau SK, Chan JF. Coronaviruses: emerging and re-emerging pathogens in humans and animals. Virol J; 22;12:209.

11. Perlman S, Netland J. Coronaviruses post-SARS: update on replication and pathogenesis. Nat Rev Microbiol. 2009;7(6):439-50.

12. Li W, Shi Z, Yu M, Ren W, Smith C, Epstein JH, et al. Bats are natural reservoirs of SARS-like coronaviruses. Science. 2005 Oct 28;310(5748):676-9.

13. Shi Z, Hu Z. A review of studies on animal reservoirs of the SARS coronavirus. Virus research. 2008;133(1):74-87.

14. Islam H, Rahman A, Masud J, Shweta DS, Araf Y, Ullah MA, et al. A Generalized Overview of SARS-CoV-2: Where Does the Current Knowledge Stand? Electron J Gen Med. 2020;17(6):em251.

15. Stadler K, Masignani V, Eickmann M, Becker S, Abrignani S, Klenk HD, et al. SARS-beginning to understand a new virus. Nat Rev Microbiol. 2003;1(3):209-18.

16. Hui DS, I Azhar E, Madani TA, Ntoumi F, Kock R, Dar O, et al. The continuing 2019-nCoV epidemic threat of novel coronaviruses to global health-The latest 2019 novel coronavirus outbreak in Wuhan, China. Int J Infect Dis. 2020;91:264-6.

17. Sarkar B, Ullah MA, Johora FT, Taniya MA, Araf Y. Immunoinformatics-guided designing of epitope-based subunit vaccines against the SARS Coronavirus-2 (SARS-CoV-2). Immunobiol. 2020;225(3):151955.

18. Ullah M, Moin AT, Araf Y, Bhuiyan AR, Griffiths MD, Gozal D. Potential Effects of the COVID-19 Pandemic on Future Birth Rate. Front Public Health. 2020;8:893.

19. Wu F, Zhao S, Yu B, Chen YM, Wang W, Song ZG, et al. A new coronavirus associated with human respiratory disease in China. Nature. 2020; 579(7798):265-269.

20. Liu X, Zhang B, Jin Z, Yang H, Rao Z. The crystal structure of 2019-nCoV main protease in complex with an inhibitor N3; doi: 10.2210/PDB6LU7/PDB

21. Xue X, Yang H, Shen W, Zhao Q, Li J, Yang K, et al. Production of authentic SARS-CoV Mpro with enhanced activity: application as a novel tag-cleavage endopeptidase for protein overproduction. J Mol biol. 2007;366(3):965-75.

22. Yang H, Bartlam M, Rao Z. Drug design targeting the main protease, the Achilles' heel of coronaviruses. Curr Pharm Des. 2006;12(35):4573-90.

23. Anderson J, Schiffer C, Lee SK, Swanstrom R. Viral protease inhibitors. In Antiviral strategies. Handb Exp Pharmacol. 2009;189(189):85-110.

24. Bernstein FC, Koetzle TF, Williams GJ, Meyer Jr EF, Brice MD, Rodgers JR, et al. The Protein Data Bank: A computer-based archival file for macromolecular structures. J Mol Biol. 1977;80(2):319-24.

25. Schrödinger Release 2018-4: Protein Preparation Wizard; Epik, Schrödinger, LLC, New York, NY, 2016; Impact, Schrödinger, LLC, New York, NY, 2016; Prime, Schrödinger, LLC, New York, NY, 2018.

26. Irwin JJ, Shoichet BK. ZINC-a free database of commercially available compounds for virtual screening. J Chem Inf Model. 2005;45(1):177-82.

27. Schrödinger Release 2018-4: LigPrep, Schrödinger, LLC, New York, NY, 2018.

28. Schrödinger Release 2018-4: Glide, Schrödinger, LLC, New York, NY, 2018.

29. Ramírez D, Caballero J. Is it reliable to use common molecular docking methods for comparing the binding affinities of enantiomer pairs for their protein target? Int J Mol Sci. 2016;17(4):525.

30. Yuriev E, Ramsland PA. Latest developments in molecular docking: 2010-2011 in review. J Mol Recognit. 2013;26(5):215-39.

31. Dassault Systèmes BIOVIA, Discovery Studio Visualizer, 19.1, San Diego: Dassault Systèmes, 2019.

32. Ullah MA, Johora FT, Sarkar B, Araf Y, Rahman MH. Curcumin analogs as the inhibitors of TLR4 pathway in inflammation and their drug like potentialities: a computer-based study. J Recept Signal Transduct Res. 2020;40(4):324-38.

33. Genheden S, Ryde U. The MM/PBSA and MM/GBSA methods to estimate ligand-binding affinities. Expert Opin Drug Discov. 2015;10(5):449-61.

34. Lyne PD, Lamb ML, Saeh JC. Accurate prediction of the relative potencies of members of a series of kinase inhibitors using molecular docking and MM-GBSA scoring. J Med Chem. 2006;49(16):4805-8.

35. Zhong H, Tran LM, Stang JL. Induced-fit docking studies of the active and inactive states of protein tyrosine kinases. J Mol Graph Model. 2009;28(4):336-46.

36. Qing X, Lee XY, De Raeymaecker J, Tame JR, Zhang KY, De Maeyer M, et al. Pharmacophore modeling: advances, limitations, and current utility in drug discovery. J Recep Ligand Channel Resear. 2014;7:81-92.

37. Khedkar SA, Malde AK, Coutinho EC, Srivastava S. Pharmacophore modeling in drug discovery and development: an overview. Med Chem. 2007;3(2):187-97.

38. Wolber G, Langer T. Ligand Scout: 3-D pharmacophores derived from protein-bound ligands and their use as virtual screening filters. J Chem Inf Model. 2005;45(1):160-9.

39. Kaserer T, Beck KR, Akram M, Odermatt A, Schuster D. Pharmacophore models and pharmacophore-based virtual screening: concepts and applications exemplified on hydroxysteroid dehydrogenases. Molecules. 2015;20(12):22799-832.

40. Wang J, Hou T. Recent advances on in silico ADME modeling. Annu Rep Comput Chem. 2009;5:101-27.

41. Sarkar B, Islam SS, Ullah MA, Hossain S, Prottoy MN, Araf Y, et al. Computational Assessment and Pharmacological Property Breakdown of Eight Patented and Candidate Drugs against Four Intended Targets in Alzheimer's Disease. Adv Biosci Biotechno. 2019;10(11):405.

42. Ullah A, Prottoy NI, Araf Y, Hossain S, Sarkar B, Saha A. Molecular Docking and Pharmacological Property Analysis of Phytochemicals from Clitoria ternatea as Potent Inhibitors of Cell Cycle Checkpoint Proteins in the Cyclin/CDK Pathway in Cancer Cells. Comput Mol Biosci. 2019;9(03):81.

43. Yang H, Lou C, Sun L, Li J, Cai Y, Wang Z, et al. admetSAR 2.0: web-service for prediction and optimization of chemical ADMET properties. Bioinformatics. 2019;35(6):1067-9.

44. Pires DE, Blundell TL, Ascher DB. pkCSM: predicting small-molecule pharmacokinetic and toxicity properties using graph-based signatures. J Med Chem. 2015;58(9):4066-72.

45. Parasuraman S. Prediction of activity spectra for substances. J Pharmacol Pharmacother. 2011;2(1):52.

46. Lagunin A, Stepanchikova A, Filimonov D, Poroikov V. PASS: prediction of activity spectra for biologically active substances. Bioinformatics. 2000;16(8):747-8.

47. Schrödinger Release 2018-4: Jaguar, Schrödinger, LLC, New York, NY, 2018.

48. Becke AD. A new mixing of Hartree–Fock and local density-functional theories. J Chem Phys. 1993;98(2):1372-7.

49. Gill PM, Johnson BG, Pople JA, Frisch MJ. The performance of the Becke-Lee-Yang-Parr (B-LYP) density functional theory with various basis sets. Chem Phys Lett. 1992;197(4-5):499-505.

50. Stephens PJ, Devlin FJ, Chabalowski CF, Frisch MJ. Ab initio calculation of vibrational absorption and circular dichroism spectra using density functional force fields. J Phys Chem. 1994;98(45):11623-7.

51. Pearson RG. Absolute electronegativity and hardness correlated with molecular orbital theory. Proc Natl Acad Sci U S A. 1986;83(22):8440-1.

52. Parr RG. Density functional theory of atoms and molecules. In Horizons of Quantum Chemistry. 1980 pp. 5-15.

53. Gschwend DA, Good AC, Kuntz ID. Molecular docking towards drug discovery. J Mol Recognit. 1996;9(2):175-86.

54. Sarkar B, Ullah A, Araf Y, Islam NN, Zohora US. Immunoinformatics-guided Designing and In Silico Analysis of Epitope-based Polyvalent Vaccines against Multiple Strains of Human Coronavirus (HCoVs). Expert Rev Vaccines. 2021.

55. Shoichet BK, McGovern SL, Wei B, Irwin JJ. Lead discovery using molecular docking. Curr Opin Chem Biol. 2002;6(4):439-46.

56. Davis AM, Teague SJ. Hydrogen bonding, hydrophobic interactions, and failure of the rigid receptor hypothesis. Angew Chem Int Ed Engl. 1999;38(6):736-49.

57. Xu T, Ooi A, Lee HC, Wilmouth R, Liu DX, Lescar J. Structure of the SARS coronavirus main proteinase as an active C2 crystallographic dimer. Acta Crystallogr Sect F Struct Biol Cryst Commun. 2005;61(11):964-6.

58. Yang SY. Pharmacophore modeling and applications in drug discovery: challenges and recent advances. Drug Discov Today. 2010;15(11-12):444-50.

59. Khedkar SA, Malde AK, Coutinho EC, Srivastava S. Pharmacophore modeling in drug discovery and development: an overview. Med Chem. 2007;3(2):187-97.

60. Wang Y, Xing J, Xu Y, Zhou N, Peng J, Xiong Z, et al. In silico ADME/T modelling for rational drug design. Q Rev Biophys. 2015;48(4):488-515.

61. Sarkar B, Ullah MA, Islam SS, Rahman MH, Araf Y. Analysis of plant-derived phytochemicals as anti-cancer agents targeting cyclin dependent kinase-2, human topoisomerase IIa and vascular endothelial growth factor receptor-2. J Recept Signal Transduct Res. 2020;12:1-7.

62. Paul Gleeson M, Hersey A, Hannongbua S. In-silico ADME models: a general assessment of their utility in drug discovery applications. Curr Top Med Chem. 2011;11(4):358-81.

63. Li AP. Screening for human ADME/Tox drug properties in drug discovery. Drug Discov Today. 2001;6(7):357-66.

64. Geerts T, Vander Heyden Y. In silico predictions of ADME-Tox properties: drug absorption. Comb Chem High Throughput Screen. 2011;14(5):339-61.

65. Anzenbacher P, Anzenbacherova E. Cytochromes P450 and metabolism of xenobiotics. Cell Mol Life Sci. 2001;58(5-6):737-47.

66. Lamb DC, Waterman MR, Kelly SL, Guengerich FP. Cytochromes P450 and drug discovery. Curr Opin Biotechnol. 2007;18(6):504-12.

67. De Graaf C, Vermeulen NP, Feenstra KA. Cytochrome P450 in silico: an integrative modeling approach. J Med Chem. 2005;48(8):2725-55.

68. Ames BN, Gurney EG, Miller JA, Bartsch H. Carcinogens as frameshift mutagens: metabolites and derivatives of 2-acetylaminofluorene and other aromatic amine carcinogens. Proc Natl Acad Sci U S A. 1972;69(11):3128-32.

69. Xu C, Cheng F, Chen L, Du Z, Li W, Liu G, et al. In silico prediction of chemical Ames mutagenicity. J Chem Inf Model. 2012;52(11):2840-7.

70. Priest B, Bell IM, Garcia M. Role of hERG potassium channel assays in drug development. Channels. 2008;2(2):87-93.

71. Hacker K, Maas R, Kornhuber J, Fromm MF, Zolk O. Substrate-dependent inhibition of the human organic cation transporter OCT2: a comparison of metformin with experimental substrates. PloS one. 2015;10(9) :e0136451.

72. Stepanchikova AV, Lagunin AA, Filimonov DA, Poroikov VV. Prediction of biological activity spectra for substances: Evaluation on the diverse sets of drug-like structures. Curr Med Chem. 2003;10(3):225-33.

73. Lagunin A, Stepanchikova A, Filimonov D, Poroikov V. PASS: prediction of activity spectra for biologically active substances. Bioinformatics. 2000;16(8):747-8.

74. Zhan CG, Nichols JA, Dixon DA. Ionization potential, electron affinity, electronegativity, hardness, and electron excitation energy: molecular properties from density functional theory orbital energies. J Phys Chem A. 2003;107(20):4184-95.

75. Becke AD. Density-functional exchange-energy approximation with correct asymptotic behavior. Phys Rev A Gen Phys. 1988;38(6):3098.

76. Sacan A, Ekins S, Kortagere S. Applications and limitations of in silico models in drug discovery. Methods Mol Biol. 2012;910:87-124.